Theoretical Study on the Optoelectronic Properties of Electron-Withdrawing Substituted Diethynylfluorenyl Gold(I) Complexes

Yi Liao,[†,‡,§] Guo-Chun Yang,[§] Ji-Kang Feng,*[,†,‡] Li-Li Shi,[†] Shuang-Yang Yang,[†] Li Yang,[†] and Ai-Min Ren[†]

State Key Laboratory of Theoretical and Computational Chemistry, Institute of Theoretical Chemistry, Jilin University, Changchun 130023, P. R. China, The College of Chemistry, Jilin University, Changchun 130023, P. R. China, and Institute of Functional Material Chemistry, Faculty of Chemistry, Northeast Normal University, Changchun 130024, China

Received: March 2, 2006; In Final Form: August 14, 2006

We report on a quantum-chemical study of the electronic and optical properties of gold(I) complex AuTFT (**1**) and its electron-withdrawing substitutents, AuTFOT (**2**) and AuTFCNT (**3**) [where TFT = diethynylfluorenyl, TFOT = diethynylfluorenone and TFCNT = diethynyl-(9-(dicyanomethylene)fluorene)]. Our theoretical calculations indicate that for all systems the reorganization energies of electron and hole are in the same order of magnitude and similar to those of the well-known electrontransport material Alq_3. The substitution of −CO and $-C(CN)_2$ for −CH in AuTFT significantly decreases the bond length alternation and increases the electron affinity, which would effectively lower the energy barrier for electron injection from cathode and thus qualify AuTFOT (**2**) and AuTFCNT (**3**) as candidates for the electron transport layer (ETL) in light-emitting diodes (LEDs). The lowest lying excited-states of gold(I) diethynylfluorenyl derivatives have been studied by the singles configuration interaction (CIS) method and time-dependent density functional method (TDDFT). It is found that the electron-withdrawing substitutions evidently decrease the energy gap, leading to a remarkable red shift in transition energy and transformation in the direction of charge transfer. Our research is important in the development of new functional materials for the design of LEDs with enhanced performance.

Introduction

There has been a continuing interest in the design of alkynylgold(I) complexes in the past few decades.[1] The preference of gold(I) for a linear coordination geometry, together with the linearity of the acetylide unit and its π-unsaturated nature have made the alkynylgold(I) complexes attractive building blocks for organometallic oligomeric and polymeric materials which may possess unique properties such as optical nonlinearity, electrical conductivity, and liquid crystallinity.[2] The luminescent property of gold(I) acetylide was first reported by Che in 1993[3] and has been extensively studied by Yam and Che.[4] Most recently, a new series of bis(alkynyl) gold(I) and mercury(II) complexes and polymers incorporating fluorenyl-based linking units were synthesized by Wong and co-workers.[5]

The fluorene moiety provides a rigidly planarized biphenyl structure within the molecular backbone and its substituent derivatives at the C-9 position offer the prospect of controlling material properties such as solubility, emission wavelengths, energy gap, ionization potential (IP), electron affinity (EA) and migration of charge,[6] all of which are key factors that must be considered in designing functional materials for electrical and optical applications. For LEDs, the performance of devices is directly affected by the mobilities of electrons and holes in the materials. It is desirable that the injected holes and electrons have large and similar mobilities to prevent electroluminescence quenching that can occur when charges recombine close to a metallic interface. Despite the importance of carrier injection and transport as well as the nature of luminescence, most studies in this area focus on experimental synthesis, structural analysis and spectral measurement.

Recently, quantum-chemical calculations have proven useful in gaining insight into the optoelectronic properties of organometallic compounds.[7] These theoretical calculations, approved by a wide range of experimental measurements, could well explain the process of photoexcitation or photoluminescence and the mechanism of electron transfer.[8] For commercial exploitation of this kind of alkynylgold(I) complexes and for direct application-aimed synthesis, a thorough understanding of the relationship between electronic structure and optoelectronic property is necessary. This seemed an attractive goal for us to perform detailed theoretical investigations on alkynylgold(I) complexes with electronically tunable fluorenyl linkers.

As an extension of our recent interest in d^{10} metal acetylides,[9] herein we report the studies on structural, electronic and optical properties as well as the carrier mobility of a series of alkynylgold(I) complexes [$PH_3AuC{\equiv}CRC{\equiv}CAuPH_3$] (R = electron withdrawing substituted fluorenyl groups). We anticipate that introduction of electron-withdrawing substitutents (such as cyano and carbonyl) at the C-9 position of fluorene moiety would allow the properties of gold diethynylfluorene to be fine-tuned at the molecular level. For comparison and calibration, a ligand precursor has also been examined. The molecular structures of alkynylgold(I) complexes and their free ligands are sketched in Figure 1.

* Corresponding author. Email: JiKangf@yahoo.com; Fax: +86-431-8945942.

† State Key Laboratory of Theoretical and Computational Chemistry, Institute of Theoretical Chemistry, Jilin University.

‡ The College of Chemistry, Jilin Universit.

§ Northeast Normal University.

10.1021/jp061326i CCC: $33.50
Published on Web 11/11/2006

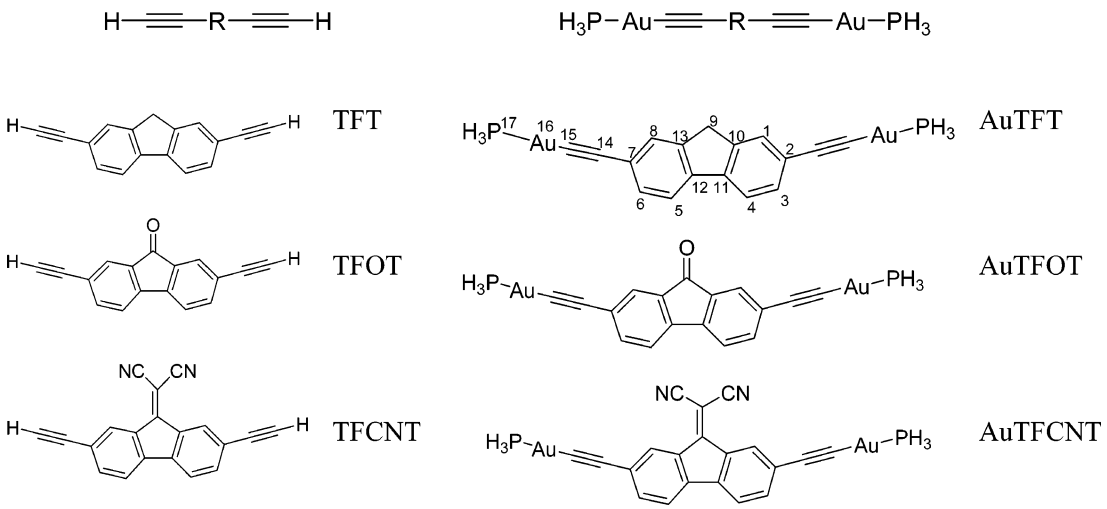

Figure 1. Sketch structures of the alkynylgold(I) complexes and corresponding free ligand, together with the abbreviations used. (The triple bonds are abbreviated by T, the fluorene rings by F, the fluorenone rings by FO and the 9-(dicyanomethylene)fluorene by FCN.)

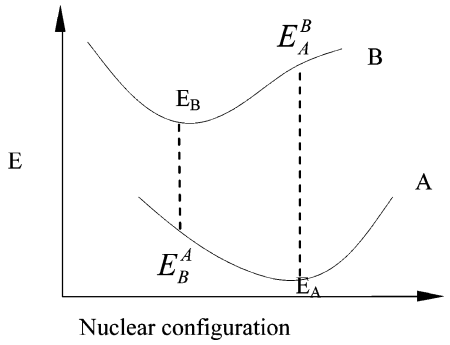

Figure 2. Schematic description of inner reorganization energy calculation.

Computational Methods

At the microscopic level, the charge transport mechanism can be described as a self-exchange transfer process, in which an electron or hole transfer occurs from one charged molecule to an adjacent neutral molecule. The rate of intermolecular charge transfer (K_{et}) can be estimated from semiclassical Marcus theory[10] given in

$$K_{et} = A \exp\left[\frac{-\lambda}{4k_B T}\right] \quad (1)$$

where T is the temperature, A is a prefactor related to the electronic coupling between adjacent molecules, λ is the reorganization energy, and K_B is the Boltzmann constant. It will be seen that variations in the reorganization energies, which have an exponential barrier (eq 1), dominate the changes in overall carrier transfer rates as the molecular structures are varied. For efficient charge transport, the reorganization energy needs to be small. At this stage, we focus our discussion on the reorganization energy.

Generally, the λ value is determined by fast changes in molecular geometry (the inner reorganization energy λ_i) and by slow variations in solvent polarization of the surrounding medium (the external contribution λ_e). In the case of LEDs (there are condensed-state systems), however, the latter contribution can be neglected, so that the former becomes the dominant factor. The inner reorganization energy λ_i, which is caused by the change of the internal nuclear coordinates from the reactant A to the product B (see Figure 2), can be evaluated as sum of two relaxation energies, i.e.

$$\lambda_i = (E_A^B - E_B) + (E_B^A - E_A) \quad (2)$$

Full geometry optimization for each molecule in their neutral, anionic and cationic states was completed using the Gaussian 03 software package[11] with the density functional theory. All open-shell calculations were performed using unrestricted methods (UDFT), and spin contamination in the radical species was found to be very small ($\langle S^2 \rangle \leq 0.77$). Recent studies show that DFT calculations are remarkably successful in predicting a wide variety of problems in organometallic chemistry.[12] Becke's three-parameter hybrid method[13] using the Lee−Yang−Parr correlation functional[14] was employed (denoted as B3LYP) here. Gradient optimizations were carried out using the 6-31G* basis set[15] for P, O, N, C and H atoms. Owing to the large number of electrons and to account for relativistic effects, the gold atom was represented by the ECP60MWB relativistic effective core potential from the Stuttgart/Bonn group (19 valence electrons) and its associated (8s7p6d)/[6s5p3d] basis set.[16] The above basis set for all atoms is abbreviated as E60.

The geometry optimizations of the lowest singlet (S_1) and triplet (T_1) excited states were performed at the level of configuration interaction considering single electron excitations (CIS)[17] from filled to unfilled molecular orbitals using the optimized ground-state geometry and were checked further by the time depemdent dnsity-functional formalism (TDDFT)[18] with the B3LYP functional in conjunction with a def-SV(P) basis set, as implemented in TURBOMOLE 5.6.[19] In a few cases the geometries of the S_2 and T_2 states were also examined.

On the basis of ground and excited-state optimization, the TD-DFT approach[20] (Gaussian03) was applied to investigate the excited-state electronic properties of alkynylgold(I) complexes at level of B3LYP/E60. This method is based on the Kohn−Sham formulation of DFT and uses the eigenvalues and eigenvectors of the Kohn- Sham equation. However, no spin−orbit interactions are included within this formulation. Recently, Wang and Ziegler[21] proposed a TDDFT formalism within the two-component relativistic zeroth-order regular approximation scheme based on the nonconllinear exchange-correlation XC functional. This formalism can deal with spin−orbit coupling SOC and recover the 3-fold degeneracy of triplet excitations. To evaluate the effect of SOC on the luminescent properties of heavy transition metal complexes of alkynylgold(I), the two-

TABLE 1: Optimized Geometries of Ground (S_0) and Excited States (S_1/T_1) as Well as Bond Length Alternation (Δr) of Gold Diethynyl Derivatives (Bond Lengths (Å))

	AuTFT			AuT(FO)T			AuT(FCN)T		
	S_0[a]	S_1[b]	T_1[b]	S_0[a]	S_1[b]	T_1[b]	S_0[a]	S_1[b]	T_1[b]
r(1,2)	1.414	1.435	1.450	1.416	1.413	1.419	1.415	1.417	1.415
r(2,3)	1.414	1.437	1.448	1.412	1.445	1.459	1.410	1.438	1.449
r(3,4)	1.392	1.380	1.373	1.398	1.380	1.373	1.396	1.377	1.372
r(4,11)	1.399	1.422	1.439	1.392	1.417	1.430	1.390	1.417	1.424
r(10,11)	1.413	1.438	1.455	1.412	1.454	1.464	1.419	1.454	1.463
r(1,10)	1.385	1.375	1.366	1.382	1.390	1.381	1.392	1.395	1.394
r(9,10)	1.517	1.517	1.521	1.501	1.473	1.482	1.481	1.456	1.457
r(11,12)	1.464[a] 1.48[c]	1.428	1.404	1.477	1.421	1.409	1.463	1.416	1.407
r(7,14)	1.426	1.403	1.398	1.425	1.415	1.409	1.425	1.413	1.411
r(14,15)	1.226[a] 1.23[c]	1.241	1.242	1.226	1.235	1.236	1.226	1.235	1.235
r(15,16)	1.981[a] 1.99[c]	1.989	1.988	1.983	1.992	1.992	1.984	1.994	1.994
r(16,17)	2.328[a] 2.28[c]	2.343	2.348	2.329	2.353	2.352	2.329	2.354	2.353
Δr	0.018	0.037	0.082	0.008	0.043	0.063	0.006	0.040	0.051

[a] B3LYP for ground states. [b] TD-B3LYP for excited states. [c] Experimental data from ref 5a.

component TDDFT formalism implemented in the ADF 2006.01 program package[22] was performed at the excited state geometries obtained above with the LB94 potential as the XC functional and the adiabatic local density approximation (ALDA) as the XC kernel. The electronic configurations of the molecular systems were described by a triple-ξ-plus-polarization (TZP) basis set, featuring Slater-type orbitals, for all atoms.

Changes in electron-density distribution upon excitation were calculated as difference electron densities between the ground state and the investigated excited state, as described by TD-DFT (Gaussian03). The difference density plots were prepared using the GaussView software. All the calculations described here were performed at the SGI Origin 3900 server.

Results and Discussion

Optimized Molecular Geometries in Ground States. The optimized geometrical parameters of the gold(I) complexes AuTFT (**1**), AuTFOT (**2**), and AuTFCNT (**3**) in their ground-state equilibrium configurations are presented in Table 1. (See Figure 1 for the numbering of atoms.) There are no published structures for compounds **1**−**3**, but there are some related structures for comparison such as those of [$Ph_3PAuC{\equiv}C-FO-C{\equiv}CAuPPH_3$] and the [$Me_3PAuC{\equiv}C-FO-C{\equiv}CAuPMe_3$].[5] Optimized structures of Au-TFT (**1**) and its derivatives **2** and **3** exhibit nearly planar geometry (angles C−Au−C, C≡C−Au and C−C≡C are close to 180°), which is in agreement with the related X-ray data,[5a] where the bigold centers adopt a two-coordinate linear geometry in a rigid-rod manner. The calculated C≡C and Au−C bond distances in Au-TFOT are 1.226 and 1.983 Å, respectively. These values are also in the same range as in the X-ray characterized bis(alkynyl) gold phosphines (1.23 and 1.99 Å).[5a]

Our theoretical calculations reveal that the introduction of the electron-withdrawing cyano and carbonyl groups connected at the C9-position of the fluorene has an effect on the bond lengths of the fluorenyl fragment whereas the remote diethynyl and gold fragments are nearly unchanged (shown in Table 1). To evaluate the relaxation of bond length upon substituent as a whole, we employ the concept of the difference between the average length of the "single" and "double" bonds (BLA). The degree of bond length alternation has been used as a structural parameter in interpreting electronic spectra of many classes of conjugated molecules.[23] In this paper, BLA is defined as follows:

$$\Delta r = (R_{C1-C2} + R_{C2-C3} + R_{C4-C11} + R_{C10-C11} + R_{C9-C10})/5 - (R_{C3-C4} + R_{C1-C10} + R_{C11-C12})/3 \quad (3)$$

It can be seen from Table 1 that, induced by the electron-withdrawing effect of the substituted groups, the bond length alternation (Δr) decreases markedly (aromaticity increase) when going from AuTFT (0.018) to carbonyl-substituted AuTFOT (0.008) and to the most strongly electronegative AuTFCNT (0.006). As known, the optical band gap in conjugated molecules originates mainly from distortion due to single/double bond length alternation. Therefore, the reducing bond length alternation along the backbone of the conjugated gold diethynylfluorenyl may decrease the band gap effectively.

Reorganization Energy, Ionization Potential and Electron Affinity. For each molecule, the geometry is also optimized in the radical-cation and anion states. The bond parameters of compounds **1**−**3** in their optimized neutral, cationic and anionic states are listed in the Supporting Information. The electron density isocontours of the HOMOs and LUMOs are shown in Figure 3. The energies corresponding to the different charged

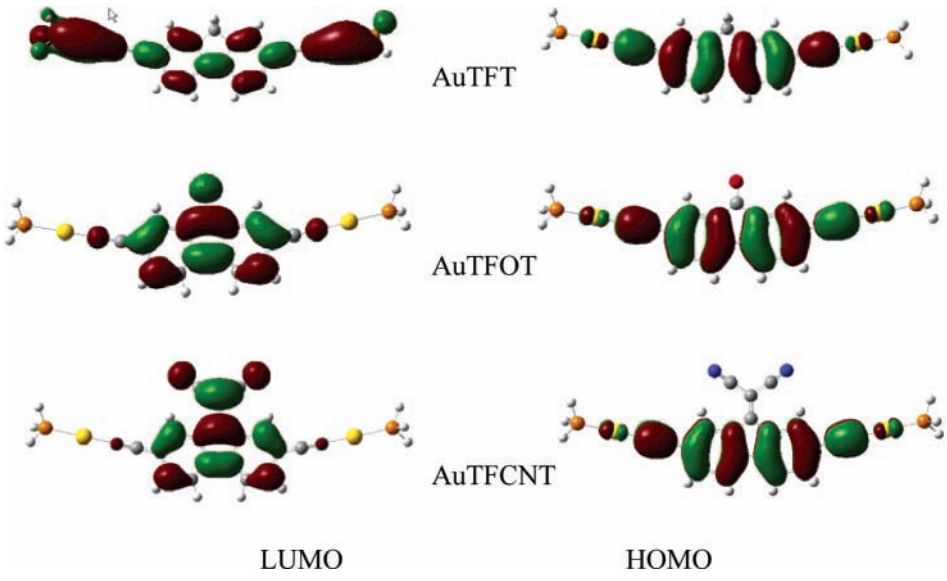

Figure 3. Contour plots of the highest occupied and lowest virtual orbitals in gold diethynyl derivatives.

states in the relevant geometries are then obtained for calculating the reorganization energies for hole and electron transport ($\lambda_{i(h)}$ and $\lambda_{i(e)}$, respectively).

Our DFT-B3LYP/E60 method gives $\lambda_{i(e)} = 0.24$, 0.27 and 0.29 eV for **1**−**3**, respectively, and the value of $\lambda_{i(h)}$ is in the same order of magnitude (0.29, 0.28 and 0.25 eV for **1**−**3**, respectively). It is noteworthy that the internal reorganization energies for electron transport ($\lambda_{i(e)}$) increase as the electron-withdrawing ability increases, whereas the improvement in electron-acceptance yields a decrease in the reorganization energies for hole transport ($\lambda_{i(h)}$). Given that the internal reorganization energy is a measure of the geometric distortion as a result of charge transfer, it may be misleading to explain λ_i by the mere presence of a particular characteristic in a series of compounds. Such different effects of the electron-withdrawing sbustituent on $\lambda_{i(h)}$ and $\lambda_{i(e)}$ should be well explained from comparison of the geometries in the neutral and charged states.

It can be seen form Supporting Information that the bonds $C_{11}-C_{12}$, C_7-C_{14} and Au−P of AuTFT undergo a significant decrease from the neutral to the radical-anion state. Unlike AuTFT, a more significant change in AuTFOT and AuTFCNT from neutral to the anionic state is mainly localized on $C_{11}-C_{12}$, $C_{10}-C_{11}$ and C_9-C_{10}. The analysis of the frontier orbitals is consistent with this picture. Note that, to a first approximation, the characteristics of the LUMO can be taken to estimate where additional negative charges will be stored. It is clear from Figure 3 that the LUMO of AuTFT is delocalized over the whole molecule except atom C_9, and the LUMOs of AuTFOT and AuTFCNT are mainly localized on the fluorenyl ring (for AuTFOT, contribution from the alkynyl fragment can be found in the LUMO). The augment in the conjugation on going from system AuTFCNT to AuTFOT and then to AuTFT provides a rationalization for the gradual decrease of $\lambda_{i(e)}$, because the extra negative charge is delocalized in longer conjugated backbone.

The HOMOs of all compounds mainly consist of the π orbital of the diethynyl fluorenyl fragment and a few metal dπ orbitals. The main structure distortions in the cation relative to the neutral molecule are consistent with this picture. For example, there is an antibonding interaction between the π orbitals on $C_{11}-C_{12}$ as well as C_7-C_{14}. Hence, removing an electron from HOMO leads to a shortening of these bond distances in the cationic state relative to the neutral state. From the above discussion, we may tentatively relate the reorganization energies $\lambda_{i(h)}$ and $\lambda_{i(e)}$ to the HOMO and LUMO, respectively. Thereby, systematic modification on the molecular level can be utilized for qualitatively adjusting reorganization energy.

In comparison with Alq_3 ($\lambda_{i(e)} = 0.28$ eV at B3LYP/6-31G* level),[24] this series of gold complexes ($\lambda_{i(e)}$: 0.24−0.29 eV) exhibit high mobilities in electron transport and may be used as electron-transport materials. In addition, for AuTFOT, the injected electrons and holes have large and similar mobilities, which is crucial in achieving a high quantum efficiency in optoelectronic devices.

It is well-known that the optoelectronic properties for OLED devices depend on balance injection and transport of electrons and holes. As mentioned above, the charge transport of the title system is determined mainly by λ_i. Although the charge injection is determined by the barriers between the IPs, EAs of the materials and the work function (Φ) of the contact electrodes. For the commonly used indium tin oxide (ITO) anode ($\Phi_a \sim$ 4.7−4.8 eV) and air-stable cathodes such as aluminum ($\Phi_c \sim$ 4.0−4.3 eV), most emissive organic materials have a larger barrier for the electron ($\Delta E_e = \Phi_c - EA$) than for hole ($\Delta E_h = \Phi_a - IP$). Therefore, looking for better electron injection molecules (high EA) is imperative for further improvement in device performance.

TABLE 2: Selected Calculated Excitation Energies (ΔE), Wavelengths (λ), Oscillator Strenghs (f) and Nature for Low-Lying Singlet (S_n) States of Substituted Gold Diethynylfluorene and Their Free Ligands

systems	state	composition		nature	ΔE(eV)/ λ(nm)	f
Au-TFT	S_1	H → L	67%	$\pi \rightarrow \pi^*$	3.18/389	1.467
	S_{10}	H → L+6	64%	$\pi \rightarrow \pi^*$	4.11/301	0.534
	S_{19}	H-2 → L+2	41%	$\sigma/\pi \rightarrow \pi^*$	4.75/261	0.510
TFT	S_1	H → L	64%	$\pi \rightarrow \pi^*$	3.96/313	1.037
Au-TFOT	S_1	H → L	66%	$\pi \rightarrow \pi^*/d_{xz} \rightarrow \pi^*$	2.61/475	0.226
	S_3	H → L+1	66%	$\pi \rightarrow \pi^*$	3.40/365	1.054
	S_{16}	H → L+7	50%	$\pi \rightarrow \pi^*$	4.36/284	1.146
		H-5 → L	35%			
	S_{27}	H-2 → L+3	45%	$\sigma/\pi \rightarrow \pi^*$	4.83/257	0.271
TFOT	S_1	H → L	66%	$\pi \rightarrow \pi^*$	2.86/433	0.066
Au-TFCNT	S_1	H → L	68%	$\pi \rightarrow \pi^*/d_{xz} \rightarrow \pi^*$	1.90/652	0.045
	S_5	H → L+1	60%	$\pi \rightarrow \pi^*$	3.35/370	0.720
		H-5 → L	32%			
	S_7	H-5 → L	56%	$\pi \rightarrow \pi^*$	3.63/342	1.077
		H → L+1	28%			
TFCNT	S_1	H → L	68%	$\pi \rightarrow \pi^*$	2.20/563	0.017

The vertical ionization potential, IP_v, is defined here as differences in energies of cationic and neutral states at the optimized geometries for the neutral states. The vertical electron affinity, EA_v, is described as differences in energies between neutral and anionic states in the optimized neutral molecule. The calculated electronic structures (IP_v, EA_v) of AuTFOT (**2**) and AuTFCNT (**3**) are (6.32, 0.70 eV) and (6.47, 1.48 eV), respectively. As compared with AuTFT (**1**) (6.05, 0.29 eV), the substitution of an electron-withdrawing side group shows asymmetric stabilization of the HOMO and LUMO levels, which suggest that the single particle energy gap (IP − EA) follows the order AuTFT > AuTFOT > AuTFCNT, consistent with the above discussion on BLA. Moreover, it is interesting to note the EA of 1.48 eV obtained for AuTFCNT (**3**) is 2 times higher than that of AuTFOT (**2**) (0.70 eV), which in turn is 2.4 times higher than that of the AuTFT (**1**) (0.29 eV). Compared with the most widely used light emitting and electrontransport material Alq_3 ($EA_v = 0.83$ eV at B3LYP/6-31G* level),[25] AuTFCNT and AuTFOT show significant amelioration in EA, which can effectively promote the injection of the electron form cathode into devices and thus lower the turn-on voltage and improve the performance of devices.

Photoexcitation. To gain insight into the effects of electron-withdrawing substituents and metal complexation on the electronic structure and spectral properties of gold diethynylfluorenyl derivatives, we have performed TD-B3LYP calculations. The calculated excitation energies for the selected excited states of the three model systems as well as corresponding ligands in their ground-state equilibrium geometries are listed in Table 2. The contour plots for changing of electron density distribution upon $S_0 \rightarrow S_n$ excitation are presented in Figure 4. The transition assignments were based upon detailed consideration of molecular orbitals shown in Supporting Information and principal configurations from Td-B3LYP calculations. Excited states that arise from transitions between orbitals that were located on different moieties were classified as charge transfer (CT) excited states, such as ligand-to-metal charge transfer (LMCT), metal-to-ligand charge transfer (MLCT) and ligand-to-ligand charge transfer (LLCT), although those from π-occupied to π-virtual orbitals located on the same ligand were described as intraligand (IL) and those form orbitals residing on the same metal center were defined as metal-centered (MC).

For complex Au-TFT, the $S_0 \rightarrow S_1$ transition calculated at 389 nm has the largest oscillator strength of 1.467 and is mainly

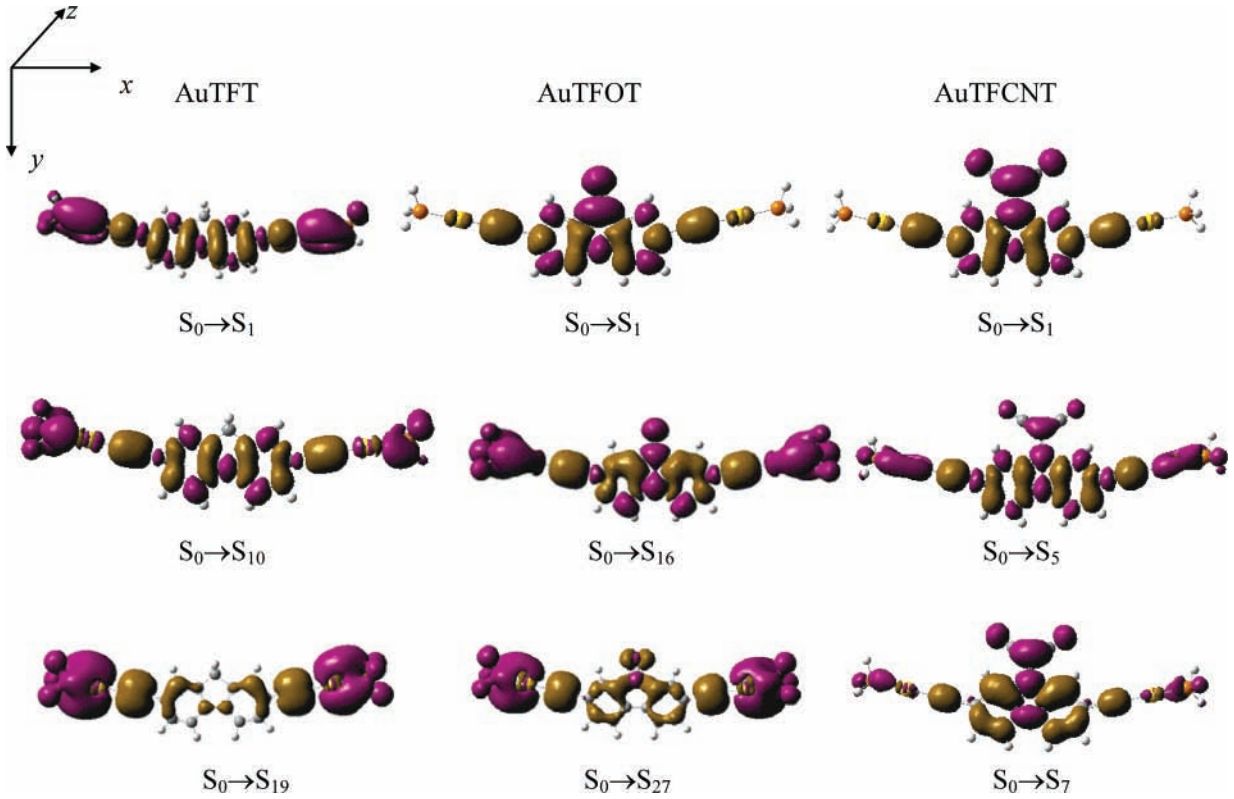

Figure 4. Change of electron density distribution upon the $S_0 \rightarrow S_n$ electronic transition of substituted gold ethynylfluorene complexes. Yellow and violet colors correspond to a decrease and increase of electron density, respectively.

associated with transition from the HOMO to the LUMO, as the coefficient in the configuration interaction wave functions is up to 0.67. As shown in Figure 3, the HOMO of AuTFT is the π bonding orbital, and the LUMO is the π^*-antibonding obital; thus the $S_0 \rightarrow S_1$ transition can be assigned as a long-axis polarized $\pi\pi^*$ transition in nature. Our assignment for AuTFT is in fair quantitative and qualitative agreement with those for other digold(I) complexes [H_3PPAuC≡CRC≡CAu-PPH_3] (R = fluorine; 9,9-dihexylfluorene), which display an intense $\pi\pi^*$ transition in the near-UV region (ca. 343−360 nm) in dichloromethane at 290 K.[5a] From Table 2 and Figure 4, the $S_0 \rightarrow S_1$ lowest energy transition for AuTFT can be characterized as a primary IL (π(fluorenyl) → π^*(fluorenyl)), LLCT (π-(C≡C) → π^*(fluorenyl)) together with LMCT (π(C≡C) → p_z(Au)), and slightly MC ($d_{xz} \rightarrow p_z$). Similar to the lowest energy transition, the second intense absorption band of AuTFT ($S_0 \rightarrow S_{10}$, $f = 0.534$), predicted at 301 nm, also corresponds to IL, LLCT and LMCT. However, different charge transfer can be observed when the molecule is excited to a higher lying excited state, such as $S_0 \rightarrow S_{19}$ (corresponds to the third intense absorption band $f = 0.51$), which has a principal configuration stemming from the H−2 → L+2 electronic transition and comprises mainly LMCT (σ(fluorenyl)/π(C≡C) → p_y(Au)). Therefore, we may deduce that during excitation the electron will transfer from the donor alkynyl bridge to the acceptor fluorenyl ring (right side) and the metal segment (left side) at a relative low energy transition; however, in a higher energy transition, the electron will transfer from the diethynylfluorenyl ring to the metal segment.

For Au-TFOT (**2**) and Au-TFCNT (**3**) (see Figure 4), although the $S_0 \rightarrow S_1$ is also HOMO → LUMO in character, the situation is considerably different. First, the oscillator strength of excitation to the S_1 state in **2** ($f = 0.20$) and **3** ($f = 0.05$) is lower than that in **1**. This is not unexpected because the π and π^* orbitals in question have little overlap (see Figure 3). Second, as the electron-withdrawing groups, carbonyl (**2**) and cyano (**3**), were introduced into the fluorenyl side chain, an obvious red shift (by 86 nm for **2** and 263 nm for **3**) could be observed in the absorption spectra as compared with that of **1**. This was attributed to the change in the relative energies of the frontier molecular orbitals. The results of DFT/B3LYP MO calculations (presented in Supporting Information) showed that the electron-withdrawing CO and greater electronegtivity CN on the fluorenyl ring stabilizes more the LUMO and less the HOMO level with respect to the unsubstituted system **1**, hence decreasing the LUMO−HOMO energy gap following the order 3.54 eV (**1**) > 3.19 eV (**2**) > 2.49 eV (**3**). Furthermore, these red-shifted lowest energy excitations in **2** and **3** arise from a different MLCT (d_{xz}(Au) → π^*(fluorenyl)) in addition to the above-mentioned IL (π(fluorenyl) → π^*(fluorenyl)) and LLCT (π(C≡C) → π^*(fluorenyl)). It is noteworthy that in **2** and **3**, this MLCT only exists in low energy absorption; the most intense transitions ($S_0 \rightarrow S_{16}$ at 296 nm (**2**); $S_0 \rightarrow S_7$ at 321 nm (**3**)) are also characterized as IL, LLCT and LMCT.

As might be expected, the absorption spectra of the ligands TFT, TFOT and TFCNT are considerably simpler than those of their metal complexes counterparts. Without perturbation from the electrophilic metal center, the lowest energy excitations of all ligands feature $\pi\pi^*$ IL and LL transition with a blue-shift transition energy relative to their corresponding complexes due to a reduction in the degree of π-delocalization through the conjugated molecule. As stated in our previous study, π-conjugation can be preserved through the d^{10} metal center due to weak interaction between metal dπ-orbital and ligand pπ-orbital.[9]

From above discussions we may infer that the metal center can effectively conjugate with the ligand part and exhibit amphoteric behavior in this series of systems. On one hand the gold and fluorenyl segment act as an electron acceptor on either side of the ethynyl donor linkage constructing (acceptor−donor-

TABLE 3: HF/E60 Ground State and CIS/E60 Excited State Bond Lengths (Å) for AuTFT, AuTFOT and AuTFCNT(Molecule Label in Figure 1)

	AuTFT			AuT(FO)T			AuT(FCN)T		
	S_0	S_1	T_1	S_0	S_1	T_1	S_0	S_1	T_1
r(1,2)	1.397	1.422	1.430	1.401	1.386	1.401	1.400	1.384	1.394
r(2,3)	1.397	1.425	1.428	1.395	1.443	1.444	1.392	1.439	1.442
r(3,4)	1.384	1.363	1.363	1.391	1.356	1.360	1.388	1.353	1.355
r(4,11)	1.386	1.419	1.427	1.379	1.419	1.420	1.377	1.417	1.419
r(10,11)	1.396	1.431	1.437	1.396	1.446	1.443	1.401	1.447	1.449
r(1,10)	1.378	1.359	1.358	1.373	1.384	1.372	1.382	1.395	1.385
r(9,10)	1.515	1.516	1.517	1.497	1.463	1.481	1.490	1.446	1.465
r(11,12)	1.471	1.409	1.407	1.484	1.398	1.409	1.470	1.390	1.397
r(7,14)	1.440	1.405	1.415	1.439	1.423	1.422	1.438	1.423	1.422
r(14,15)	1.205	1.219	1.213	1.204	1.208	1.209	1.204	1.207	1.208
r(15,16)	2.024	2.017	2.022	2.025	2.026	2.026	2.027	2.030	2.029
r(16,17)	2.382	2.377	2.380	2.382	2.382	2.382	2.382	2.383	2.382
Δr	0.007	0.066	0.072	0.002	0.052	0.057	0.001	0.047	0.055

acceptor) the ADA structure. When the electron-withdrawing groups cyano and carbonyl were introduced into the fluorenyl ring, the metal fragment transforms to a weak electron donor and readily couples to fluorenyl acceptor units via the alkynyl donor bridge, re-forming a donor−acceptor (DA) structure. Such DA architectures with improved intramolecular charge transfer can facilitate manipulation of the electronic structure (such as HOMO−LUMO levels, EA and IP), leading to small band gap semiconducting materials or materials with rich optoelectronic properties, as confirmed by our calculation.

Photoluminescence. To simulate the emission spectra of the investigated materials, we have explored the geometrical relaxation phenomena taking place in the lowest lying excited state. CIS (single configuration interaction) has been extensively used to study these problems;[26] it describes the excited-state wave function at a level comparable to Hartree−Fock. Using the CIS method for geometries and TD-DFT for excitation energies might cause inconsistent results in the evaluation of the Stokes shifts. By a recently developed TD-DFT gradient method,[18] it is now possible to optimize the geometry of individual singlet or triplet excited states. To establish the quality of the CIS calculations, the geometries of excited states were also optimized at the level of TD-DFT.

In Table 3, we present the calculated S_1 and T_1 geometrical parameters of AuTFT, AuTFOT and AuTFCNT at the CIS/E60 level of theory. For comparison, HF/E60 ground-state geometries are also collected in Table 3. The TD-DFT excited-state geometries and corresponding DFT ground-state geometries are collected in Table 1.

From Tables 1 and 3, it is clear that the optimized S_1/T_1 geometrical structures from both methods have similar changing trends as compared with their corresponding ground state geometries (CIS: HF and TDDFT: DFT). First, pronounced geometrical modification is manifested in the diethynylfluorene fragment rather than in the metal fragment, the latter appears to be extremely rigid with respect to electron excitation. Furthermore, more prominent modifications are found to be centralized on the fluorene ring in the diethynylfluorene ligand than in the ethynyl part. Second, the enhancement in the bond-length alternation on going from S_0 to S_1 and then to T_1 in all systems leads to the appearance of a quinoid geometric character on the excited states of the fluorene ring. For example, Δr (defined in formula **3**) for AuTFT increased from ∼0.007 Å in the ground state (HF) to ∼0.066 Å in the singlet excited state (CIS) and to ∼0.072 Å in the triplet state (CIS). The larger bond length alternation in T_1 with respect to S_1 is in accordance with the larger relaxation energies in T_1 (0.31 eV) than S_1 (0.29 eV) upon vertical excitation. Also in this case the relaxation of the structures during the excitation can be interpreted in terms of the antibonding and bonding character of the highest occupied molecular orbital (HOMO) and lowest unoccupied molecular orbital (LUMO), respectively. In fact, according to TD-DFT the S_1 state is essentially described by a HOMO → LUMO transition and this leads to slightly shorter single bonds and longer double bonds. From Figure 3 we may see the LUMO has nodes across the C_1-C_2, C_2-C_3, C_4-C_{11}, $C_{10}-C_{11}$, C_9-C_{10} and $C_{14}-C_{15}$ bonds, but the HOMO is bonding in these regions. Therefore, one would expect elongation of these bonds. Table 3 shows that these bonds are in fact considerably longer in the excited state and present quinoid character. The HOMO has a node across the C_3-C_4, C_1-C_{10}, $C_{11}-C_{12}$ and C_7-C_{14} bond whereas the LUMO is bonding. The data in Table 3 confirm the anticipated contraction of these bonds.

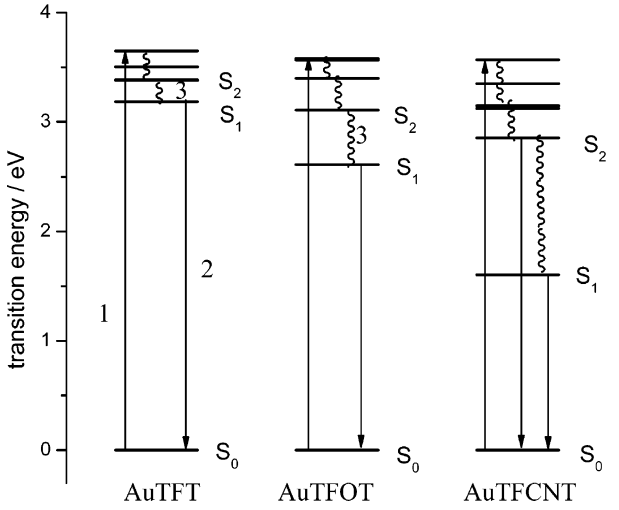

Figure 5. Schematic drawing of electronic energy levels and photophysical processes in AuTFT, AuTFOT and AuTFCNT: (1) excitation; (2) fluorescence; (3) internal conversion. (The relative ground-state S_0 is chosen as the reference point.)

On the basis of the CIS and TD-DFT optimized excited states geometries, the fluorescence and phosphoresce emission energies of AuTFT, AuTFOT and AuTFCNT are evaluated at the TD-B3LYP/E60 level. According to the empirical Kasha's rule,[27] the luminescence of isolated systems commonly originates from the radiative decay of the lowest excited state. Thus, the photophysical properties of compounds are governed by their first singlet (S_1) and/or triplet (T_1) excited state. However, there may be an exception to this rule, such as in system AuTFCNT. Figure 5 shows the calculated vertical transition energy level of all systems. Note that a relatively large energy gap between S_1 and S_2 exists in AuTFCNT. Generally, a larger energy gap between the lowest and the next lowest excited-state tends to reduce the internal conversion and thus enhance the emission from the higher electronic state. Therefore, the second excited states (S_2 and T_2) of AuTFCNT are also taken into account when interpreting the nature of luminescence in gold(I) diethynylfluorenyl complexes.

Table 4 presents the calculated emission wavelengths for gold diethynylfluorenyl derivatives at TD-B3LYP//CIS level. For intuition, a graphical display of illustrating $S_1/T_1 \rightarrow S_0$ electronic transition is shown in Figure 6 (for AuTFCNT, $S_2/T_2 \rightarrow S_0$ are also included). The emission wavelengths from the TD-B3LYP//TD-B3LYP calculation are presented in Supporting Information Table S3.

From Tables 4 and S3, it is clear that the TDDFT//CIS calculations provide results very similar to those from the TDDFT//TDDFT calculations. Both methods give uniform

TABLE 4: Calculated Fluorescence and Phosphorescence Wavelengths (λ) and Their Transition Nature for Gold Diethynylfluorenyl Derivatives at the TD-B3LYP/E60//CIS/E60 Level

systems	state	composition		nature	$\Delta E(eV)/\lambda(nm)$	f
Au-TFT	S1	H ← L	65%	$\pi\pi^*$	2.98/416	1.62
	T1	H ← L	72%	$\pi\pi^*$	1.98/626	0.00
Au-TFOT	S1	H ← L	65%	$\pi\pi^*/d_{xz}\pi^*$	2.09/593	0.22
	T1	H ← L	78%	$\pi\pi^*$	1.49/830	0.00
Au-TFCNT	S1	H ← L	65%	$\pi\pi^*/ d_{xz}\pi^*$	1.42/870	0.05
	S2	H-1←L	68%	$\pi\pi^*/ d_{xz}\pi^*$	2.95/421	0.01
	T1	H ← L	77%	$\pi\pi^*$	1.12/1102	0.00
	T2	H-2 ← L	85%	$\pi\pi^*$	1.61/776	0.00

designation in the nature of the excited state. The deviation of fluorescence wavelengths between two methods is within 12 nm; oscillator strengths vary by no more than 0.01. Despite the overall good agreement, an intending difference occurs between TDDFT//CIS and TDDFT//TDDFT results regarding the phosphorescence wavelengths, which are larger by 87−190 nm according to our TDDFT//TDDFT calculations. These initial investigations suggest that the TDDFT//CIS level of theory should be capable of reproducing the emission wavelength with a modest stock shift as the TDDFT//TDDFT method.

The emissions from the lowest excited states in the gold(I) complexes closely resemble those of the absorption maximum with a red shift in energy and lower oscillator strength, supporting the assignment of the lowest energy excited state to be the metal-perturbed $\pi\pi^*$ intraligand (fluorenyl) and LL (fluorenyl → C≡C) transition. The increase in the emission maximum passing from AuTFT to AuTFOT and to AuTFCNT is attributed to the presence of the electron-withdrawing substituents, CO and CN, which are electronegative and give a more delocalized π-system and, hence, a significantly lower energy of the first excited state. In all gold(I) complexes, AuTFCNT has the lowest S_0-S_1 energy gap of 1.42 eV, which is even lower than the S_1-S_2 gap of 1.43 eV (see Table 3). Thus, the second excited states of AuTFCNT may have some contribution to the luminescence. According to our calculations, the S_2 of Au-TFT, predicted at 421 nm, is described by the L → H−1 excitation and mainly corresponds to LLCT (fluorenyl → C≡C) and LMCT (π(fluorenyl) → d_{xz}(Au)); T_2 of AuTFCNT is dominated by a L → H−2 transition, which can be characterized as a $\pi\pi^*$IL (fluorenyl), whereas the second triplet excited state should have no contribution to phosphorescence because of a relatively lower $T_1 - T_2$ gap (0.5 eV) to $S_0 - T_1$ gap (1.12 eV).

It should be pointed out that the TDDFT results presented above do not provide information on triplet−singlet emission intensities because SOC effects are not included. Spin−orbit coupling can mix singlet and triplet states, allowing the latter to acquire intensity in both absorption and emission. The two-component TDDFT formalism is used here to evaluate the contributions to the emission in terms of singlet and triplet single group scalar relativistic excited states. The transition energies from two-component and scalar relativistic TDDFT calculations for alkynylgold(I) complexes are listed in Supporting Information Table S4.

From Table S4, it can be seen that the emission energies obtained from two-component TDDFT (with SOC) are in fair quantitative agreement with those from scalar TDDFT (without SOC). The trivial impact of SOC on emission energies of

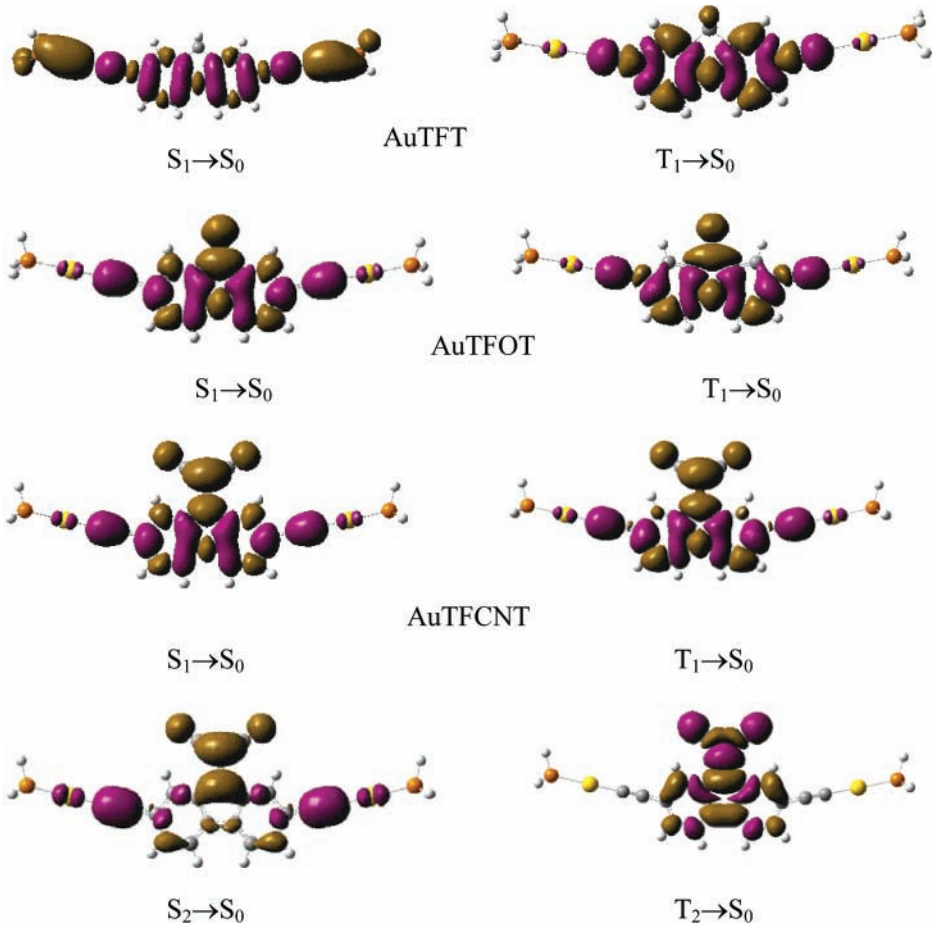

Figure 6. Change of electron density distribution upon the $S_n/T_n \rightarrow S_0$ electronic transition of substituted gold ethynylfluorene complexes. Yellow and violet colors correspond to a decrease and increase of electron density, respectively.

alkynylgold(I) complexes can be rationalized by the fact that the orbitals involved in the lowest energy transitions from our ADF calculations have tiny contribution from Au 5d and 6p components, limited spin−orbit splitting of which is considered the reason for such a similar transition shown in Table S4. From our discussion, it is clear that the TDDFT results without SOC should still provide a reasonable description of the overall orbital excitations for this series of alkynylgold(I) complexes.

Conclusion

A comprehensive photophysical study has been carried out on the gold diethynylfluorenyl complexes AuTFT, AuTFOT and AuTFCNT (where TFT = diethynylfluorenyl, TFOT = diethynylfluorenone and TFCNT = diethynyl-(9-(dicyanomethylene)-fluorine). The objective of this work is to determine the effect of the metal complexation and the electron-withdrawing substituent on the properties of excited states. The calculated results indicate that the incorporation of the metal center introduces more sublevels into the energy hierarchy, which permits complicated electronic transitions to take place, and hence diverse electronic properties can be tuned by subtle modification, such as the electron-withdrawing substituent CO and CN change the direction of electron transfer from LMCT in AuTFT to MLCT (in AuTFOT and AuTFCNT) during $S_0 \rightarrow S_1$ transition. Moreover, the spectra data also display that the electron-withdrawing substituent may effectively decrease the energy gap, leading to a red shift in maximum absorption and emission relative to those of unsubstituted AuTFT.

To evaluate the potential application of these gold complexes to the OLED, the charge injection and transfer ability is assessed in terms of IP, EA and internal reorganization energy, respectively. Based on our calculation, the reorganization energy for hole transport $\lambda_{i(h)}$ is related to the HOMO and the reorganization energy for electron transport $\lambda_{i(e)}$ is controlled by the LUMO. The values of $\lambda_{i(e)}$ in this series of gold complexes vary from 0.24 to 0.29 eV, and the values of $\lambda_{i(h)}$ have a similar range of 0.25−0.29 eV, which are comparable with those of well-known electrontransport and luminescent material Alq_3 ($\lambda_{i(h)} = 0.24$ eV and $\lambda_{i(e)} = 0.28$ eV at B3LYP/6-31G* level).[24] Although the carbonyl and cyano substituents in AuTFOT and AuTFCNT slightly improve the reorganization energy for electron transport relative to that of AuTFT, the withdrawing effect of carbonyl and cyano groups can effectively improve the electron affinity and lower the barrier for electron injuection, rendering the material n-conducting. We may expect that AuTFOT and AuTFCNT would be promising candidates of electrontransport materials in LEDs.

In summary, our present work clearly demonstrates that the modification of the conjugated molecule backbone with electron-deficient carbonyl- and dicyano-substituted electron acceptors in the side chain was found to be effective for tuning the optoelectronic properties of this class of materials.

Acknowledgment. This work is supported by the Major State Basis Research Development Program (973, 2002CB-613406) and Youth Science Foundation of Northeast Normal University (111494018).

Supporting Information Available: Table S1 list B3LYP/E60 calculated structures of **1**−**3** in their neutral, cationic and anionic state; Molecular orbital components of gold diethynylfluorenyl derivatives are presented in Table S2; Table S3 shows calculated fluorescence and phosphorescence wavelengths for gold diethynylfluorenyl derivatives at the TD-B3LYP/E60//TD-B3LYP/def-SV(P) level; transition energies from two-component and scalar relativistic TDDFT calculations for alkynylgold(I) complexes are listed in Table S4. This material is available free of charge via the Internet at http://pubs.acs.org.

References and Notes

(1) (a) McArdle, C. P.; Irwin, M. J.; Jennings, M. C.; Puddephatt, R. J. *Angew. Chem., Int. Ed. Engl.* **1999**, *38*, 3376−3378. (b) Méndez, L. A.; Jiménez, J.; Cerrada, E.; Mohr, F.; Laguna, M. *J. Am. Chem. Soc.* **2005**, *127*, 852−853. (c) Puddephatt, R. J. *Chem. Commun*. **1998**, 1055−1062. (d) Irwin, M. J.; Jia, G. C.; Payne, N. C.; Puddephatt, R. J. *Organometallics* **1996**, *15*, 51−57.

(2) (a) Whittall, I. R.; Humphrey, M. G.; Samoc, M.; Luther-Davies, B. *Angew. Chem., Int. Ed. Engl*. **1997**, *36*, 370−371. (b) Whittall, I. R.; McDonagh, A. M.; Humphrey, M. G.; Samoc, M. *Adv. Organomet. Chem.* **1999**, *43*, 349−405. (c). Whittall, I. R.; Humphrey, M. G.; Houbrechts, S.; Persoons, A.; Hockless, D. C. R. *Organometallics* **1996**, *15*, 5738−5745. (d) Alejos, P.; Coco, S.; Espinet, P. *New J. Chem.* **1995**, *19*, 799−805.

(3) Li, D.; Hong, X.; Che, C. M.; Lo, W. C.; Peng, S. M. *J. Chem. Soc., Dalton Trans.* **1993**, 2929−2932.

(4) (a) Yam, V. W. W.; Choi, S. W. K. *J. Chem. Soc., Dalton Trans.* **1996**, 4227−4232. (b) Chao, H. Y.; Lu, W.; Li, Y.; Chan, M. C. W.; Che, C. M.; Cheung, K. K.; Zhu, N. *J. Am. Chem. Soc.* **2002**, *124*, 14696−14706. (c) Lu, W.; Xiang, H. F.; Zhu, N.; Che, C. M. *Organometallics* **2002**, *21*, 2343−2346. (d) Che, C. M.; Chao, H. Y.; Miskowski, V. M.; Li, Y.; Cheung, K. K. *J. Am. Chem. Soc.* **2001**, *123*, 4985−4991.

(5) (a) Wong, W. Y.; Choi, K. H.; Lu, G. L.; Shi, J. X.; Lai, P. Y.; Chan, S. M. *Organometallics* **2001**, *20*, 5446−5454. (b) Wong, W. Y.; Liu, L.; Shi, J. X. *Augew. Chem. Int. Ed*. **2003**, *42*, 4064−4068. (c) Wong, W. Y.; Liu, L.; Poon, S. Y.; Choi, K. H.; Cheah, K. W.; Shi, J. X. *Macromolecules* **2004**, *37*, 4496−4504.

(6) (a) Fukuda, M.; Sawada, K.; Yoshino, K. *J. Polym. Sci., Part A* **1993**, *31*, 2465−2471. (b) Klaener, G.; Miller, R. D. *Macromolecules* **1998**, *31*, 2007−2009. (c) Greczynski, G.; Fahlman, M.; Salaneck, W. R. *Chem. Phys. Lett.* **2000**, *321* 379−384.

(7) (a) Koentjoro, O. F.; Rousseau, R.; Low, P. J. *Organometallics* **2001**, *20*, 4502−4509. (b) Makedonas, C.; Mitsopoulou, C. A.; Lahoz, F. J.; Balana, A. I. *Inorg. Chem*. **2003**, *42*, 8853−8865. (c) Batista, E. R.; Martin, R. I. *J. Phys. Chem. A* **2005**, *109*, 3128−3133. (d) Urtel, H.; Bikzhanova, G. A.; Grotjahn, D. B.; Hofmann, P. *Organometallics* **2001**, *20*, 3938−3949. (e) Iron, M. A.; Martin, J. M. L.; Van der Boom, M. E. *J. Am. Chem. Soc*. **2003**, *125*, 11702−11709.

(8) (a) Stoyanov, S. R.; Villegas, J. M.; Rillema, D. P. *Inorg. Chem*. **2003**, *42*, 7852−7860. (b) Boulet, P.; Chermett, H.; Daul, C.; Gilardoni, F.; Rogemond, F.; Weber, J.; Zuber, G. *J. Phys. Chem. A* **2001**, *105*, 885−894. (c) Li, J.; Djurovich, P. I.; Alleyne, B. D.; Yousufuddin, M.; Ho, N. N.; Thomas, J. C.; Peters, J. C.; Bau, R.; Thompson, M. E. *Inorg. Chem*. **2005**, *44*, 1713−1727.

(9) Liao, Y.; Feng, J. K.; Yang, L.; Ren, A. M. *Organometallics* **2005**, 24, 385.

(10) (a) Marcus, R. A. *J. Chem. Phys.* **1965**, *24*, 966−978. (b) Marcus, R. A. *Rev. Mod. Phys.* **1993**, *65*, 599−610.

(11) Frisch, M. J.; Trucks, G. W.; Schlegel, H. B.; Scuseria, G. E.; Robb, M. A.; Cheeseman, J. R.; Montgomery, J. A., Jr.; Vreven, T.; Kudin, K. N.; Burant, J. C.; Millam, J. M.; Iyengar, S. S.; Tomasi, J.; Barone, V.; Mennucci, B.; Cossi, M.; Scalmani, G.; Rega, N.; Petersson, G. A.; Nakatsuji, H.; Hada, M.; Ehara, M.; Toyota, K.; Fukuda, R.; Hasegawa, J.; Ishida, M.; Nakajima, T.; Honda, Y.; Kitao, O.; Nakai, H.; Klene, M.; Li, X.; Knox, J. E.; Hratchian, H. P.; Cross, J. B.; Adamo, C.; Jaramillo, J.; Gomperts, R.; Stratmann, R. E.; Yazyev, O.; Austin, A. J.; Cammi, R.; Pomelli, C.; Ochterski, J. W.; Ayala, P. Y.; Morokuma, K.; Voth, G. A.; Salvador, P.; Dannenberg, J. J.; Zakrzewski, V. G.; Dapprich, S.; Daniels, A. D.; Strain, M. C.; Farkas, O.; Malick, D. K.; Rabuck, A. D.; Raghavachari, K.; Foresman, J. B.; Ortiz, J. V.; Cui, Q.; Baboul, A. G.; Clifford, S.; Cioslowski, J.; Stefanov, B. B.; Liu, G.; Liashenko, A.; Piskorz, P.; Komaromi, I.; Martin, R. L.; Fox, D. J.; Keith, T.; Al-Laham, M. A.; Peng, C. Y.; Nanayakkara, A.; Challacombe, M.; Gill, P. M. W.; Johnson, B.; Chen, W.; Wong, M. W.; Gonzalez, C.; Pople, J. A. *Gaussian 03*, revision B.04; Gaussian, Inc.: Pittsburgh, PA, 2003.

(12) (a) Ziegler, T. *Chem. Rev*. **1991**, *91*, 651−667. (b) Niu, S.; Hall, M. B. *Chem. Rev*. **2000**, *100*, 353−405. (c) Li, S.; Hall, M. B. *Organometallics* **2001**, *20*, 2153-2160. (d) Conner, D.; Jayaprakash, K. N.; Cundari, T. R.; Gunnoe, T. B. *Organometallics* **2004**, *23*, 2724−2733.

(13) Becke, A. D. *J. Chem. Phys*. **1993**, *98*, 5648−5652.

(14) (a) Lee, C.; Yang, W.; Parr, R. G. *Phys. Rev. B* **1988**, *37*, 785−789. (b) Miehlich, B.; Savin, A.; Stoll, H.; Preuss, H. *Chem. Phys. Lett*. **1989**, *157*, 200−206.

(15) Hariharan, P. C.; Pople, J. A. *Theor. Chim. Acta* **1973**, *28*, 213−222.

(16) Andrae, D.; Haeussermann, U.; Dolg, M.; Stoll, H.; Preuss, H. *Theor. Chim. Acta* **1990**, *77*, 123−141.

(17) (a) Foresman, J. B.; Head-Gordon, M.; Pople, J. A.; Frisch, M. J. *J. Phys. Chem*. **1992**, *96*, 135−149. (b) Foresman, J. B.; Frisch, A. E. *Exploring Chemistry with Electronic Structure Methods*, 2nd ed.; Gaussian Inc.: Pittsburgh, PA, 1995; Chapter 8, p 213.

(18) (a) Van Caillie, C.; Amos, R. D. *Chem. Phys. Lett.* **1999**, *308*, 249−255. (b) Van Caillie, C.; Amos, R. D. *Chem. Phys. Lett.* **2000**, *317*, 159−164. (c) Furche, F.; Ahlrichs, R. *J. Chem. Phys.* **2002**, *117*, 7433−7447.

(19) Ahlrichs, R.; Bär, M.; Baron, H.-P.; Bauernschmitt, R.; Böcker, S.; Ehrig, M.; Eichkorn, K.; Elliot, S.; Haase, F.; Häser, M. Horn, H.; Huber, C.; Huniar, U.; Kattannek, M.; Kölmel, C.; Kollwitz, M.; Ochsenfeld, C.; Öhm, H.; Schäfer, A.; Schneider, U.; Treutler, O.; von Arnim, M.; Weigend, F.; Weis, P.; Weiss, H. *TURBOMOLE*, version 5.6; Quantum Chemistry Group, University of Karlsruhe: Karlsruhe, Germany, 2002.

(20) (a) Casida, M. K.; Jamorski, C.; Casida, K. C.; Salahub, D. R. *J. Chem. Phys*. **1998**, *108*, 4439−4449. (b) Stratmann, R. E.; Scuseria, G. E. *J. Chem. Phys*. **1998**, *109*, 8218−8224.

(21) (a) Wang, F.; Ziegler, T. *J. Chem. Phys.* **2005**, *122*, 204103. (b) Wang, F.; Ziegler, T. *J. Chem. Phys.* **2005**, *123*, 194102.

(22) (a) te Velde, G.; Bickelhaupt, S. J. A.; Gisbergen, V.; Fonseca Guerra, C.; Baerends, E. J.; Snijders, J. G.; Ziegler, T. *J. Comput. Chem.* **2001**, *22*, 931−967. (b) Guerra, C. F.; Snijders, J. G.; te Velde, G.; Baerends, E. J. *Theor. Chem. Acc.* **1998**, *99*, 391−403. (c) ADF2006.01, SCM, Theoretical Chemistry, Vrije Universiteit, Amsterdam, The Netherlands, http://www.scm.com.

(23) (a) Marder, S. R.; Perry, J. W.; Bourhill, G.; Gorman, C. B.; Tiemann, B. G.; Mansour, K. *Science* **1993**, *261*, 186. (b) Marder, S. R.; Perry, J. W.; Tiemann, B. G.; Gorman, C. B.; Gilmour, S.; Biddle, S. L.; Bourhill, G. *J. Am. Chem. Soc.* **1993**, *115*, 2524−2526.

(24) Lin, B. C.; Cheng, C. P.; You, Z. Q.; Hsu, C. P. *J. Am. Chem. Soc.* **2005**, *127*, 66−67.

(25) Martin, R. L.; Kress, J. D.; Campbell I. H.; Smith, D. L. *Phys. Rev. B* **2000**, *61*, 15804−15811.

(26) (a) Zhang, J. P.; Frenking, G. *J. Phys. Chem. A* **2004**, *108*, 10296−10301. (b) Tirapattur, S.; Belletête, M.; Leclerc, M.; Durocher, G. *J. Mol. Struct. (THEOCHEM)* **2003**, *625*, 141−148. (c) Sugimoto, M.; Sakaki, S.; Sakanoue, K.; Newton, M. D. *J. Appl. Phys.* **2001**, *90*, 6092−6097. (d) Gahungu, G.; Zhang, J. P. *J. Phys. Chem. B* **2005**, *109*, 17762−17767.

(27) (a) Pope, M.; Swenberg, C. *Electronic Processes in Organic Materials*; Oxford University Press: New York, 1982. (b) Pope, M.; Swenberg, C. E. *Electronic Processes in Organic Crystals and Polymers*; Oxford University Press: New York, 1999.